THE JOURNAL OF BIOLOGICAL CHEMISTRY VOL. 290, NO. 16, pp. 10460–10471, April 17, 2015

The Structure of the Atypical Killer Cell Immunoglobulin-like Receptor, KIR2DL4*

Received for publication, September 16, 2014, and in revised form, February 10, 2015 Published, JBC Papers in Press, March 10, 2015, DOI 10.1074/jbc.M114.612291

Shoeib Moradi[‡1], Richard Berry[‡§1,2], Phillip Pymm[‡], Corinne Hitchen[‡], Simone A. Beckham[‡], Matthew C. J. Wilce[‡], Nicholas G. Walpole[‡], Craig S. Clements[‡], Hugh H. Reid[‡], Matthew A. Perugini[¶], Andrew G. Brooks[‖], Jamie Rossjohn[‡§3], and Julian P. Vivian[‡§4]**

*From the [‡]Department of Biochemistry and Molecular Biology, School of Biomedical Sciences, and the [§]Australian Research Council Centre of Excellence for Advanced Molecular Imaging, Monash University, Clayton, Victoria 3800, Australia, the [¶]Department of Biochemistry, La Trobe Institute for Molecular Science, La Trobe University, Melbourne Victoria 3086 Australia, the [‖]Department of Microbiology and Immunology, Peter Doherty Institute for Infection and Immunity, University of Melbourne, Parkville, Victoria 3010, Australia, and the **Institute of Infection and Immunity, Cardiff University, School of Medicine, Heath Park, Cardiff CF14 4XN, United Kingdom*

Background: KIR2DL4 is an important natural killer cell receptor with properties distinct from other KIRs.
Results: The D0 domain of KIR2DL4 drove self-association of the receptor.
Conclusion: Among KIRs, the self-association of KIR2DL4 is unique and a result of discrete differences in its D0 domain.
Significance: The self-association of KIR2DL4 has implications for its unique signaling and function.

The engagement of natural killer cell immunoglobulin-like receptors (KIRs) with their target ligands, human leukocyte antigen (HLA) molecules, is a critical component of innate immunity. Structurally, KIRs typically have either two (D1-D2) or three (D0-D1-D2) extracellular immunoglobulin domains, with the D1 and D2 domain recognizing the α1 and α2 helices of HLA, respectively, whereas the D0 domain of the KIR3DLs binds a loop region flanking the α1 helix of the HLA molecule. KIR2DL4 is distinct from other KIRs (except KIR2DL5) in that it does not contain a D1 domain and instead has a D0-D2 arrangement. Functionally, KIR2DL4 is also atypical in that, unlike all other KIRs, KIR2DL4 has both activating and inhibitory signaling domains. Here, we determined the 2.8 Å crystal structure of the extracellular domains of KIR2DL4. Structurally, KIR2DL4 is reminiscent of other KIR2DL receptors, with the D0 and D2 adopting the C2-type immunoglobulin fold arranged with an acute elbow angle. However, KIR2DL4 self-associated via the D0 domain in a concentration-dependent manner and was observed as a tetramer in the crystal lattice by size exclusion chromatography, dynamic light scattering, analytical ultracentrifugation, and small angle x-ray scattering experiments. The assignment of residues in the D0 domain to forming the KIR2DL4 tetramer precludes an interaction with HLA akin to that observed for KIR3DL1. Accordingly, no interaction was observed to HLA by direct binding studies. Our data suggest that the unique functional properties of KIR2DL4 may be mediated by self-association of the receptor.

Natural killer (NK)[5] cells are cytotoxic lymphocytes that are a vital component of the innate immune system. NK cells have been implicated in the control of viral infections, including HIV, herpes viruses, and poxviruses (1), together with malignancies, including acute myeloid leukemia and neuroblastoma (2, 3). Activation of NK cells is determined by the interplay between inhibitory and activating signals transduced from an array of cell surface receptors that include the killer cell immunoglobulin-like receptor (KIR) family in humans.

Classification of KIRs is based on whether they contain two or three extracellular immunoglobulin domains (KIR2D or KIR3D) as well as on the nature of the signaling domains ("L" is inhibitory, and "S" is activating). Previous studies have elucidated the structures of KIR2Ds with a D1-D2 domain arrangement (4–9) and of KIR3DL1 that has a D0-D1-D2 configuration (10). The D1 and D2 domains of KIR2Ds and KIR3DL1 recognize HLA in much the same manner, with the D1 sitting atop the α1 domain and the D2 atop the α2 domain of the HLA molecule. The D0 domain of KIR3DL1 acted as an "innate sensor" contacting the highly conserved loop between the β1 and β2 stands of the peptide-binding groove of the HLA molecule (10–12). The activating KIRs lack cytoplasmic signaling motifs but have a charged lysine residue in the transmembrane region that facilitates pairing with DAP12, a disulfide-linked immunoreceptor tyrosine-based activation motif-containing adaptor protein (13). Inhibitory KIRs have immunoreceptor tyrosine-based inhibition motifs in their cytoplasmic domains that upon engagement with ligand recruit the protein-tyrosine phosphatases SHP-1 and SHP-2 to transduce inhibitory signals (14).

KIR2DL4 is an atypical KIR that differs from the other family members in manner of cellular localization, ligand specificity, signaling, and structure. Structurally, KIR2DL4 is distinct from

* This work was supported by Australian Research Council (ARC) Grant DE130101504 and by National Health and Medical Research Council (NHMRC) of Australia Grant 1046685.
The atomic coordinates and structure factors (code 3WYR) have been deposited in the Protein Data Bank (http://wwpdb.org/).
[1] Both authors contributed equally to this work.
[2] Supported by NHMRC Peter Doherty Fellowship GNT1035636.
[3] Supported by an NHMRC Australia Fellowship. To whom correspondence may be addressed. E-mail: Jamie.rossjohn@monash.edu.
[4] Supported by an ARC DECRA Fellowship. To whom correspondence may be addressed. E-mail: Julian.vivian@monash.edu.

[5] The abbreviations used are: NK, natural killer; KIR, natural killer cell immunoglobulin-like receptor; HSPG, heparan sulfate proteoglycan; SAXS, small angle x-ray scattering; SEC, size-exclusion chromatography; MALS, multi-angle light scattering; r.m.s., root mean square.

other KIR (except KIR2DL5) in that the D1 domain is absent; instead it has a D0-D2 domain architecture (similar to KIR2DL5). Uniquely, KIR2DL4 has both inhibitory and activating signaling domains (15). Namely, KIR2DL4 contains a single cytoplasmic immunoreceptor tyrosine-based inhibition motif domain as well as a basic arginine residue in the transmembrane domain. However, instead of coupling with DAP12, KIR2DL4 recruits the FcεR-γ chain to transduce stimulatory signals (16). Further, unlike other KIRs, which signal from the plasma membrane, KIR2DL4 signals predominantly from endosomes (17).

The confirmed ligands for KIRs are HLA-class Ia molecules. Specifically, KIR2DL1/2/3 recognize HLA-C (18), KIR3DL1 binds HLA-Bw4 (19), and KIR3DL2 binds HLA-A3 and HLA-A11 (20). Despite the high level of sequence identity to their inhibitory counterparts, the ligands for many activating KIRs are unclear. KIR2DL4 is unusual in that it does not appear to interact with HLA class Ia (pHLA-Ia). Instead, cellular assays have indicated an interaction with the HLA class Ib molecule HLA-G, a monomorphic antigen-presenting molecule that resembles HLA-Ia molecules (17, 21, 22). However, whether KIRDL4 binds HLA-G remains unclear (23, 24). Indeed, recent work has suggested that KIR2DL4 can bind heparin and heparanated proteoglycans (HSPG) distinct from HLA-G (25). Further, the binding of HSPG was shown to be modulated by the D0 domain of KIR2DL4 and to affect endosomal uptake of the receptor. However, the physiological significance of this interaction is not well defined.

Here we describe the crystal structure of KIR2DL4. In keeping with its unusual functional characteristics, KIR2DL4 oligomerizes in a concentration-dependent manner, a feature not seen in other members of the KIR family to date. The oligomerization interface was formed by the association of D0 domains via residues that have been previously identified as important for KIR3DL1 binding to HLA. This suggests that the D0 domain of the KIR2DL4 tetramer does not recognize HLA in the same manner as the D0 domain of KIR3Ds. Furthermore, no interaction was observed between KIR2DL4 and a panel of 100 pHLA-Ia by single antigen bead assay nor to HLA-G by surface plasmon resonance. The data herein cast new light on the unique functional properties of KIR2DL4 and the degree to which they may be driven by self-association of the receptor.

EXPERIMENTAL PROCEDURES

Cloning and Expression of KIR2DL4—The extracellular domains of KIR2DL4*001 (residues 1–195) and the mutants F34A, W56A, F77A, and W85A were subcloned into vectors for insect cell and mammalian cell expression. For insect cell expression, the genes were subcloned into a modified baculoviral pFastBac expression vector (Invitrogen) containing a secretion signal peptide sequence and an N-terminal hexahistidine tag (26). For generating tetramers of KIR2DL4, a similar pFastBac construct was generated for the wild-type KIR2DL4 with a secretion signal peptide sequence, an N-terminal hexahistidine tag, and a C-terminal BirA tag. Similarly, for mammalian expression, the residues 1–295 and the mutants F34A, W56A, F77A, and W85A were subcloned into the pHLSec expression vector containing a secretion signal peptide sequence and an N-terminal hexahistidine tag (27). Insect cell expression of KIR2DL4 was performed by baculoviral infection of BTI-TN-5B1–4 cells (Hi-5 cells, Invitrogen). Mammalian expression was performed by transient transfection of HEK293S GnTI$^-$ cells as detailed by Aricescu *et al.* (27). From both cell lines, the KIR2DL4 was secreted into the expression medium and then dialyzed into 10 mM Tris, pH 8.0, 500 mM NaCl (buffer 1). The protein was then purified by binding to nickel-Sepharose resin in buffer 1 with 30 mM imidazole, pH 8.0, washed in buffer 1 with 30 mM imidazole, pH 8.0, and eluted with buffer 1 with 30 mM imidazole, pH 8.0, and 50 mM EDTA. KIR2DL4 was then purified by size exclusion chromatography (S200 16/60 column, GE Healthcare) in buffer 1. The yield of KIR2DL4 from insect cells was 0.5 mg/liter, which was utilized for analytical ultracentrifugation, small angle x-ray scattering, size exclusion, and multiangle light scattering experiments. However, the insect cell material was not amenable to crystallization. The yield of KIR2DL4 expressed in HEK293S GnTI$^-$ cells was 0.02 mg/liter. The material produced in mammalian cells was used in x-ray crystallography studies following overnight incubation at 298 K with 200 units of the deglycosidase endoglycosidase H (New England Biolabs).

Analytical Ultracentrifugation—Sedimentation experiments of KIR2DL4 (0.017–0.15 mg/ml) dissolved in 10 mM Tris, 150 mM NaCl, pH 8.0, were performed using a Beckman model XL-I analytical ultracentrifuge equipped with a photoelectric optical absorbance system. Sample (380 μl) and reference (400 μl) solutions were loaded into a conventional double sector quartz cell and mounted in a Beckman An-60 Ti rotor. The samples were then centrifuged at 40,000 rpm at a temperature of 293 K. Data were collected at a single wavelength (268 nm) in continuous mode without averaging using a step size of 0.003 cm. Solvent density (1.0047 g/ml at 293 K) and viscosity (1.0182 centipoise) as well as estimates of the partial specific volume, $\bar{\nu}$ (0.7208 ml/g at 293 K), were computed using the program SEDNTERP (57). Sedimentation velocity data at multiple time points were fitted to a continuous size distribution model (28–30) using the program SEDFIT (58).

Single HLA-Antigen Bead Assay—HLA class I recognition by KIR2DL4 was assessed through binding of KIR2DL4 tetramers to beads coated with a panel of 100 HLA class I A, B, and C allotypes (LabScreen HLA class I single antigen bead screen (One Lambda, Canoga Park, CA)). 5 μg of phycoerythrin-labeled KIR2DL4 tetramer was incubated with the beads for 30 min at room temperature in the dark in phosphate-buffered 300 mM NaCl (PBS-300) with 5% fetal calf serum (Ausgenex). The beads were then washed three times in PBS-300 with 0.05% Tween 20 and resuspended in PBS-300. Binding was measured on a Luminex platform (LABScan™ 100 (One Lambda)) through identification of the individual HLA allotypes via unique bead labeling and detection of the fluorescent intensity of the tetramer on each bead set. Normalized fluorescent values for analysis were obtained using the HLA Fusion software suite (One Lambda), which subtracted background using the formula,

$$\text{Normalized fluorescent value} = (S\#N - SNC\ bead) - (BG\#N - BGNC\ bead) \quad \text{(Eq. 1)}$$

where *S#N* represents sample-specific fluorescent value (trimmed mean) for bead *#N*, *SNC bead* is the sample-specific fluorescent value for negative control (nude) bead, *BG#n* is the background negative control fluorescent value for bead *#N*, and *BGNC bead* is the background negative control fluorescent value for negative control bead.

Negative control samples were obtained using unconjugated streptavidin PE in place of KIR tetramer. The experiments were performed in triplicate.

Cloning and Expression of HLA—The extracellular domains of HLA-G*01:01 and HLA-B*57:01 (residues 1–275) and β_2-microglobulin were cloned into the pET-30(b) expression vector for overexpression in *E. coli* as described previously (31, 32). The HLA and β_2-microglobulin were expressed into inclusion bodies separately in *E. coli*, refolded, and purified, as described previously (31, 32). Briefly, 60 mg of both the HLA-G and HLA-B*57:01 were refolded by rapid dilution in a solution containing 100 mM Tris-HCl, pH 8.0, 400 mM L-arginine-HCl, 5 mM reduced glutathione, and 0.5 mM oxidized glutathione (and 4 M urea for HLA-B*57:01) in the presence of 20 mg β_2-microglobulin and 10 mg of synthetic peptide. HLA-G was refolded with the RIIPRHLQL and RLPKDFRIL peptides, and HLA-B*57:01 was refolded with the LSSPVTKSF peptide. The refolded peptide·HLA·β_2-microglobulin complexes were purified by anion exchange on a diethylaminoethylcellulose column followed by size exclusion chromatography (S200 16/60 column, GE Healthcare), followed by an additional high resolution anion exchange chromatography step (Mono Q 5/5 column, GE Healthcare).

Surface Plasmon Resonance—The interaction between the extracellular domains of KIR2DL4 and HLA-G and HLA-B*57:01 was analyzed by surface plasmon resonance using a BIAcore 3000 system (GE Healthcare). All experiments were performed at 298 K. Two independent experiments were performed in separate buffers. The buffer comprised either 10 mM HEPES (pH 7.4), 300 mM NaCl, and 0.005% surfactant P20 (HBS-P20) or 10 mM sodium citrate (pH 5.5), 300 mM NaCl, and 0.005% P20 (CBS-P20). The monoclonal anti-His_6 antibody 4D11 (Thermo Scientific) was immobilized on adjacent flow cells of a CM5 Sensorchip (GE Healthcare) by amine coupling to a surface density of ~1000 resonance units. His_6-tagged KIR2DL4 was captured by the immobilized antibody. An adjacent flow cell to which KIR2DL4 was not added was activated and quenched in the same manner and served as a control cell. HLA-G and the negative control HLA-B*57:01 were serially diluted in either HBS-P20 or CBS-P20 (0.5–300 μM) and injected simultaneously over the test and control surfaces at a flow rate of 5 μl/min, with measurements taken in duplicate. The experiment was also conducted in reverse. Here, the monoclonal anti-HLA antibody W6/32 was immobilized as above, and HLA-G and the negative control HLA-B57:01 were captured on the surface. The KIR2DL4 was serially diluted as above, and the experiment was performed as above. The integrity of the analytes was confirmed by the binding of the monoclonal antibodies W6/32 to HLA by surface plasmon resonance (33) and mAb 33 to KIR2DL4 by an enzyme-linked immunosorbent assay (ELISA) (34).

Enzyme-linked Immunosorbent Assay—Direct ELISA screening of mAb 33 (34) binding to KIR2DL4 and the negative control KIR2DL2 was performed by the standard protocol (35) on Maxisorb Nunc Immunoplates (Nunc, Roskilde, Denmark). The plates were coated with 2.5 μg/well of recombinant KIR2DL4 or KIR2DL2 diluted in phosphate-buffered saline.

Small Angle X-ray Scattering—For SAXS data collection, KIR2DL4 (0.3–5 mg/ml) and KIR2DL2 (0.35–1.5 mg/ml) were prepared in 10 mM citrate, pH 5.5, plus 0.3 M NaCl. To prevent the formation of disulfide-linked dimers, a low concentration of DTT (1 mM) was added to KIR2DL4 samples. This did not adversely impact the fold (as judged by circular dichroism spectroscopy) or the ability of KIR to oligomerize (data not shown). SAXS data were collected at the SAXS/WAXS beamline of the Australian synchrotron using a 1 M Pilatus detector. Samples and matching buffer solutions were loaded into 96-well plates, and multiple 1-s exposures were collected and compared with each other to assess for radiation damage. Data were collected to cover momentum transfer intervals of $0.0097\ \text{Å}^{-1} < q < 0.6\ \text{Å}^{-1}$ for KIR2DL4 and $0.0044\ \text{Å}^{-1} < q < 0.26\ \text{Å}^{-1}$ for KIR2DL2. The modulus of the momentum transfer is defined as $q = 4\pi\sin(\theta/\lambda)$, where 2θ is the scattering angle and λ is the wavelength. Scattering images were integrated, averaged, and calibrated against water using beamline-specific software. Scattering from the buffer and empty capillaries was subtracted after scaling scattering intensities to correspond to incident beam intensities. Molecular mass was calculated by extrapolating scattering intensity at zero angle, $I(0)$, following calibration using water. Data quality was assessed on the basis of the linearity of Guinier plots, and the R_g and the pairwise intraparticle distance distribution function were determined using GNOM (36). *Ab initio* models were generated using DAMMIF (37) using *P*2 symmetry. At least 10 independent DAMMIF runs were aligned, combined, and filtered to generate a final model that retained the most consistent features using the DAMAVER package. The normalized spatial discrepancies between individual models were 0.673–0.996 (dimer) and 0.512–0.871 (tetramer). High resolution models of KIR2DL2 and 2DL4 were fitted within *ab initio* models using DAMAVER.

Size Exclusion-coupled Multiangle Light Scattering (SEC-MALS)—SEC-MALS was used to estimate the molecular masses of the KIR2DL4 samples. KIR2DL4 was prepared to a final concentration of 3, 5, and 10 mg/ml. 100 μl of each sample was subjected to SEC-MALS at a flow rate of 0.5 ml/min using a WTC030s5 column in 10 mM sodium citrate, pH 5.5, 300 mM NaCl. The system comprised a Shimadzu DGU-$20A_5$ degasser, LC-20AD liquid chromatograph, SIL-$20A_{HT}$ autosampler, CBM-20A communications bus module, SPD-20A UV-visible detector, and CTO-20AC column oven, coupled to a Wyatt Technology Corp. DAWN HELEOS-II light scattering detector and an Optilab T-rEX refractive index detector. A WyattQELS detector had been installed in the DAWN HELEOS-II at a 90° angle, replacing detector number 12. Normalization was performed against bovine serum albumin, and data collection and analysis were performed with ASTRA6 (Wyatt Technology Corp.).

Crystallization, Data Collection, Structure Determination, and Refinement—KIR2DL4 expressed in mammalian HEK 293S cells was concentrated to 4 mg/ml and crystallized at 294 K by the hanging drop vapor diffusion method from a solution comprising 10–16% PEG 3350, 4% tacsimate, pH 6.0. The crystals typically grew as plates with dimensions 0.1 × 0.1 × 0.02 mm in 7 days. Before data collection, the crystals were equilibrated in crystallization solution with 35% PEG 3350 added as a cryoprotectant and then flash-cooled in a stream of liquid nitrogen at 100 K. A 2.8 Å resolution data set was collected at the MX2 beamline (Australian Synchrotron, Victoria). The data were recorded on a Quantum-315 CCD detector and were integrated and scaled using MOSFLM and SCALA from the CCP4 program suite (38–40). Details of the data processing statistics are summarized in Table 1. The crystal structure was solved by molecular replacement, as implemented in PHASER (41), with KIR2DS4 used as the search model (Protein Data Bank accession number 3H8N (6)). The asymmetric unit contained two copies of KIR2DL4. Refinement of the model proceeded with iterative rounds of manual building in COOT (42) and refinement in PHENIX (43), with strict 2-fold non-crystallographic symmetry applied. The final model comprised residues 7–195 and an *N*-acetylglucosamine group at Asn^{118}. The sugar groups at position 152 could not be accurately modeled and were therefore excluded from the final model. The structure was validated with MOLPROBITY (44). Refinement statistics are summarized in Table 1. Coordinates and structure factors were deposited in the PDB under accession 3WYR.

TABLE 1
Data collection and refinement statistics

Parameter	Value
Data collection statistics	
Temperature (K)	100
X-ray source	MX2 Australian synchrotron
Space group	$P42_12$
Cell dimensions (Å)	$a = 87.8$, $b = 87.8$, $c = 106.0$
Resolution (Å)	50-2.8 (2.90-2.80)[a]
Total no. of observations	21,500 (2068)
No. of unique observations	10,753 (1034)
Multiplicity	2.0 (2.0)
Data completeness (%)	100 (100)
$1/\sigma_I$	10.8 (2.2)
R_{merge}[b]	0.059 (0.333)
Refinement statistics	
Non-hydrogen atoms	
Protein	2943
ligands	67
R_{factor}[2]	0.211
R_{free}[2]	0.243
r.m.s. deviation from ideality	
Bond lengths (Å)	0.003
Bond angles (degrees)	0.72
Ramachandran plot	
Favored regions (%)	94.0
Allowed regions (%)	6.0
B-Factors (Å^2)	
Wilson	49.1
Average protein	53.4
Average ligand	66.2

[a] Values shown in parentheses are for the highest resolution shell.
[b] $R_{merge} = \Sigma_{hkl} \Sigma_j |I_{hkl,j} - \langle I_{hkl} \rangle| / \Sigma_{hkl} \Sigma_j I_{hkl,j}$.
[c] $R_{factor} = \Sigma_{hkl} ||F_o| - |F_c|| / \Sigma_{hkl} |F_o|$ for all data excluding the 5% that comprised the R_{free} used for cross-validation.

RESULTS

Overall Structure of KIR2DL4

The structure of the extracellular domain of KIR2DL4, comprising residues 7–195, was resolved to 2.8 Å and refined to final R_{work} and R_{free} values of 21.1 and 24.3%, respectively (Table 1 and Fig. 1*A*). The asymmetric unit of the crystal contained two copies of KIR2DL4, each comprising two C2-type immunoglobulin (Ig) domains, the D0 domain and the D2 domain, arranged with an acute elbow angle (Fig. 1*A*).

The D0 Ig domain contained eight β-strands, with a three-stranded β-sheet comprising strands A, B, and E sandwiched against the five-stranded β-sheet comprising strands A′, C, C′, F, and G. The D0 domain had two 3_{10} helices, one connecting the C and C′ strands and the other connecting the E and F strands (Fig. 1*A*). The D2 Ig domain contained 10 β-strands and differed from the D0 domain topology with an additional short D strand. Further, linking the D0 and D2 domains was an additional F′ strand on the D2 domain that formed a sheet with the F strand of the D0 domain (Fig. 1*A*) (45).

The D2 domains within the asymmetric unit were highly similar, aligning with an r.m.s. deviation of 0.5 Å (over Cα positions 101–195). By contrast, the D0 domains aligned with an r.m.s. deviation of 1.2 Å (over Cα positions 7–97) with a notable deviation in the conformation of the loop between the C and C′ strands (5.6 Å) (Fig. 1*B*). These structural differences within the D0 domains were concomitant with a 1.2° difference in the interdomain angle between the D0 and D2 domains, with an angle of 82.3° in copy 1 and 83.5° in copy 2 (Fig. 1*B*).

KIR2DL4 had two glycosylation sites, at positions Asn^{118} and Asn^{152}, both located on the D2 domain (Fig. 1*A*). The glycosylation at Asn^{152} was conserved across KIR genes, whereas the Asn^{118} was only partially conserved and is absent from KIR3DL1 (Fig. 1*C*).

KIR2DL4 has an unusual disulfide pairing in the D0 domain. The canonical disulfide bond between residues Cys^{28} and Cys^{74} (linking the B and F strands), present in the structure of KIR3DL1 and conserved in the sequences of all other D0-containing KIRs, was absent in the crystal structure of KIR2DL4 (Fig. 1*C*). This disulfide bond is replaced by a disulfide bond linking the A and B strands between Cys^{10} and Cys^{28} (Fig. 2*A*). The tripartite arrangement of Cys^{10}, Cys^{28}, and Cys^{74} could conceivably form three separate disulfide bond configurations. However, only one configuration was observed. Among KIRs, the presence of a Cys at position 10 is unique to KIR2DL4 (Leu^{10} in other KIRs) and is conserved in KIR2DL4 sequences across primate species. This correlation suggests that Cys^{10} may play an important role in the conformation of the D0 domain. Indeed, comparison with KIR3DL1 revealed that the shift in Cys^{28} upon binding to Cys^{10} was coincident with conformational movements of Phe^{37} and Phe^{55} that directly impacted the conformation of the B, C, and C′ strands (Fig. 2*B*).

The Tetramer Interface

Unlike all known KIR structures, the oligomeric assembly of KIR2DL4 observed in the crystal lattice was tetrameric. The tetramer was generated through crystallographic symmetry (Fig. 2, *C* and *D*). The tetramer comprised two dimers, the translational dimer as observed in the asymmetric unit and the rotational dimer generated by crystallographic symmetry (Fig.

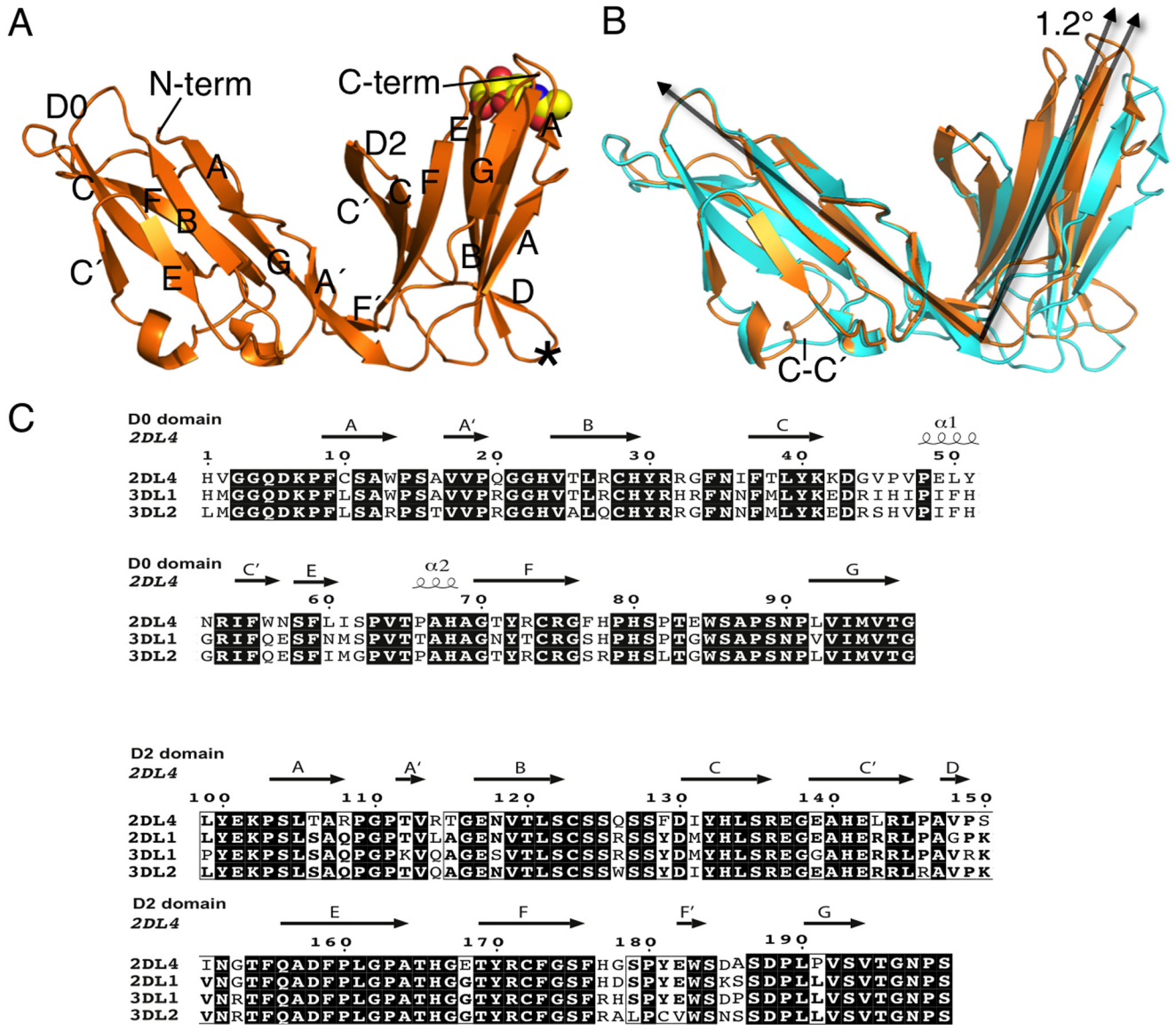

FIGURE 1. **Overall structure of KIR2DL4.** *A*, schematic representation of the monomeric KIR2DL4. The secondary structure elements are *labeled*. The position of the *N*-acetylglucosamine at position 118 is indicated as a *space-filling model*. The unmodeled *N*-acetylglucosamine at position 152 is indicated with an *asterisk*. *B*, superposition of the two copies of KIR2DL4 in the asymmetric unit (*orange* and *cyan*). The two copies deviate by 1.2° about the hinge angle of the domains. *C*, sequence alignment of the D0 and D2 domains of KIR2DL4 with KIR2DL1, KIR3DL1, and KIR3DL2.

2, *C* and *D*). The interface of the tetramer was dominated by residues in the D0 domain.

The translational dimer buried a total surface area of ~1400 Å^2, of which ~1080 Å^2 (77%) is contributed by the D0 domain (Fig. 2*D*). The D0 domains were arranged head-to-tail with the A and A′ strands and their interconnecting loop of one D0 domain packing against the C strand and the F-G loop of the other D0 domain (Fig. 3*A*). Interestingly, the A strand residues Phe^9, Ser^{11}, and Trp^{13} that were previously shown to be important in KIR3DL1 binding to HLA-B*57:01 (10) were integral to this interface, clustering with Thr^{38}, Tyr^{40}, Pro^{82}, Thr^{83}, and Trp^{85} on the opposing protomer's C strand (Fig. 3*A*). There were three hydrogen bonds at this interface, two between the D0 domains (Tyr^{51} Oη–Ser^{62} Oη and Arg^{75} Nϵ–Pro^{14} O) and one between the D2 domains (Tyr^{181} Oη–Arg^{171} Nη2) as well as a salt bridge linking the D0 and D2 domains, Arg^{73}–Glu^{137} (Fig. 3*A*). Accordingly, this interface was predominantly formed through VDW contacts. Similarly, the rotational dimer buried a total surface area of ~1110 Å^2 entirely contributed by the D0 domains. This interface contained no hydrogen bonds and was formed through a symmetric clustering of hydrophobic residues (Fig. 3*B*). Specifically, Phe^{34}, Ile^{36}, Arg^{53}, Ile^{54}, Phe^{77}, and Pro^{79} spanning the B-C, C-C′, C′-E, and F-G loops formed a large hydrophobic cluster with their symmetry counterparts (Fig. 3*B*). Flanking this central core were Phe^{77} and Trp^{85} on the interconnecting loop between the F and G strands that packed against Trp^{56} on the C′-E loop (Fig. 3*B*). Together, the tetramer interface was extensive, burying a total surface area of 4550 Å^2 and displayed good shape complementarity of 0.6 (46). Mutational experiments at the tetramer interface (F34A, W56A, F77A, and W85A) resulted in aggregated protein (data not shown). This suggests that residues at the interface and the self-association of KIR2LD4 are important to the stability of the protein.

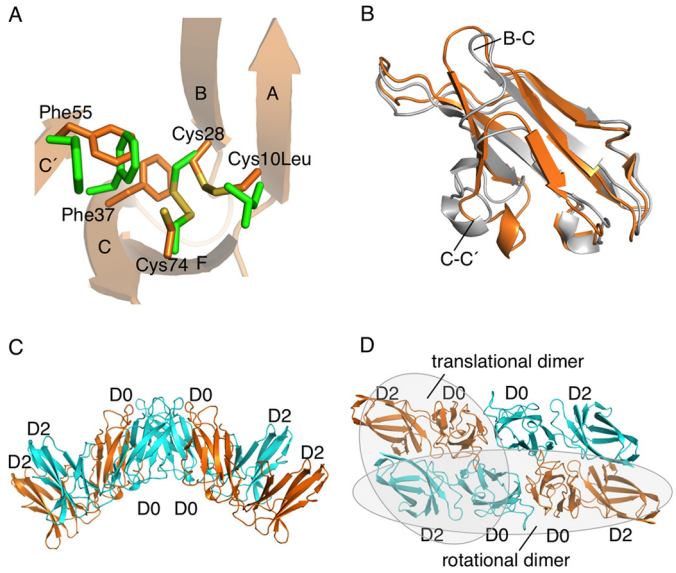

FIGURE 2. **Comparison of D0 domains from KIR2DL4 and KIR3DL1.** *A*, the trio of cysteines in KIR2DL4 D0 domain (*orange*) overlaid with the equivalent position in KIR3DL1 (*green*). The effect of the disulfide exchange on the residues Phe[37] and Phe[55] on the C and C′ strands is shown. *B*, superposition of the D0 from KIR2DL4 (*orange*) with that from KIR3DL1 (*gray*). *Labeled* are the major points of deviation at the B-C and C-C′ loops. *C*, KIR2DL4 tetramer formed by crystallographic symmetry. *D*, decomposition of the KIR2DL4 tetramer into rotational and translational dimers.

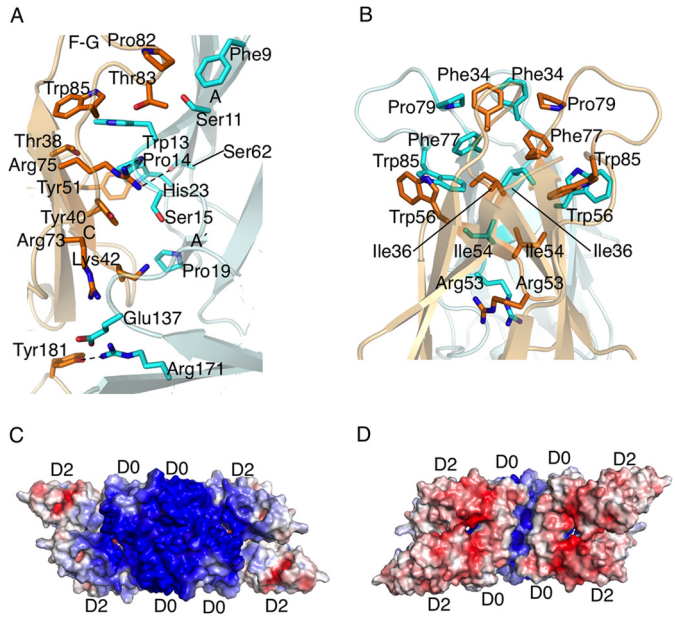

FIGURE 3. **Residues at the interface of the tetramer and mapping of electrostatic potential to the surface of KIR2DL4.** *A*, residues at the translational dimer interface. Residues on each subunit of the dimer are *colored orange* and *cyan*, respectively. *B*, residues at the rotational dimer interface. Residues on each subunit of the dimer are *colored orange* and *cyan*, respectively. *C*, the membrane proximal surface potential is predominantly electropositive (*blue*) due to the charge on the D0 domains. *D*, the membrane distal surface potential is predominantly electronegative (*red*) due to the charge on the D2 domains.

In order to determine whether the recombinant KIR2DL4 tetramer was comparable with physiological KIR2DL4, we measured binding to mAb 33 by ELISA. mAb 33 has been previously shown to recognize KIR2DL4 *in vivo* (34). The mAb 33 bound KIR2DL4 in a concentration-dependent manner and did not bind to the control KIR2DL2 (data not shown). Thus, this antibody that recognizes intracellular KIR2DL4 also recognizes our recombinantly produced KIR2DL4, which we observe to be predominantly in tetrameric form.

The tetramerization of KIR2DL4 resulted in the grouping of charged regions to form continuous, large, charged patches on the surface of the protein (Fig. 3, *C* and *D*). The charge distribution on KIR2DL4 was dipolar, with the D0 domain carrying a large positive charge on the membrane proximal face, whereas the D2 domain displayed a negative charge on the membrane distal face (Fig. 3, *C* and *D*). This large electropositive patch is a feature of the D0 domain and is absent in other KIR2DL structures solved to data. Further, relative to the membrane, the orientation of the positively charged region on KIR2DL4 is the converse to that observed in KIR3DL1. Thus, the distribution and orientation of the charged regions are unique to KIR2DL4.

Comparison with KIR2DLs and KIR3DL1 Structures

The D0 domain of KIR2DL4 shared ~81, 83, and 85% sequence similarity with the D0 domains from KIR3DL1, KIR3DL2, and KIR2DL5, respectively. The predominant area of sequence divergence corresponded to the C-C′ loop (Figs. 1*C* and 2*B*) that was associated with the tetramer interface. Compounding this difference were substitutions at Cys[10] (discussed above) and Trp[56] (Gln) and Phe[77] (Ser) that were integral to the hydrophobic core of the oligomerization interface (Figs. 1*C* and 3*B*). These deviations at the C-C′ loop and at positions 10, 56, and 77 were conserved across primate species and are probably key determinants of the self-association. By contrast, the D2 domain shared between 88 and 90% sequence similarity across the KIR family and lacked continuous regions that were unique in sequence to KIR2DL4. Accordingly, the unique self-association of KIR2DL4 was probably a result of discrete structural alterations in the D0 domain.

The interdomain angle in KIR2DL4 more closely resembled that of the D0-D1 angle in KIR3DL1 (82.4°) than the D1-D2 angles observed in other KIR structures. Typically, the equivalent D1-D2 arrangement is more acute (ranging from 66° for KIR2DL1 to 81° for KIR2DL2). Notwithstanding the differences in the interdomain angle, the structure of the D2 domain in KIR2DL4 was conserved with that of other KIR structures (r.m.s. deviation ranging from 0.75 Å for KIR2DS4 to 0.90 Å for KIR2DL1). Interestingly, D2 residues that formed HLA contacts in KIR2DL1/2 and KIR3DL1, including the critical residues Tyr[100], Phe[176], and Glu[182] are conserved in KIR2DL4 (Fig. 1*C*).

By contrast, the structure of the D0 domain deviates significantly (r.m.s. deviation of 3.5 Å) from that of KIR3DL1. The major deviations occur at the B-C (7 Å) and C-C′ loops (12 Å). These regions are directly impacted upon by the Cys[10]–Cys[28] disulfide bond and are involved at the interface of the tetramer (Fig. 2, *A* and *B*). Furthermore, the residues on the D0 domain important for KIR3DL1 binding to HLA are instead contributing to the tetramer interface in KIR2DL4. Namely, the A strand residues Phe[9], Ser[11], and Trp[13] were shown in KIR3DL1 to bind to the β1-β2 loop of HLA, whereas in KIR2DL4 they interact with the F-G loop (residues 82–85) at the tetramer interface (Fig. 3*A*). Further-

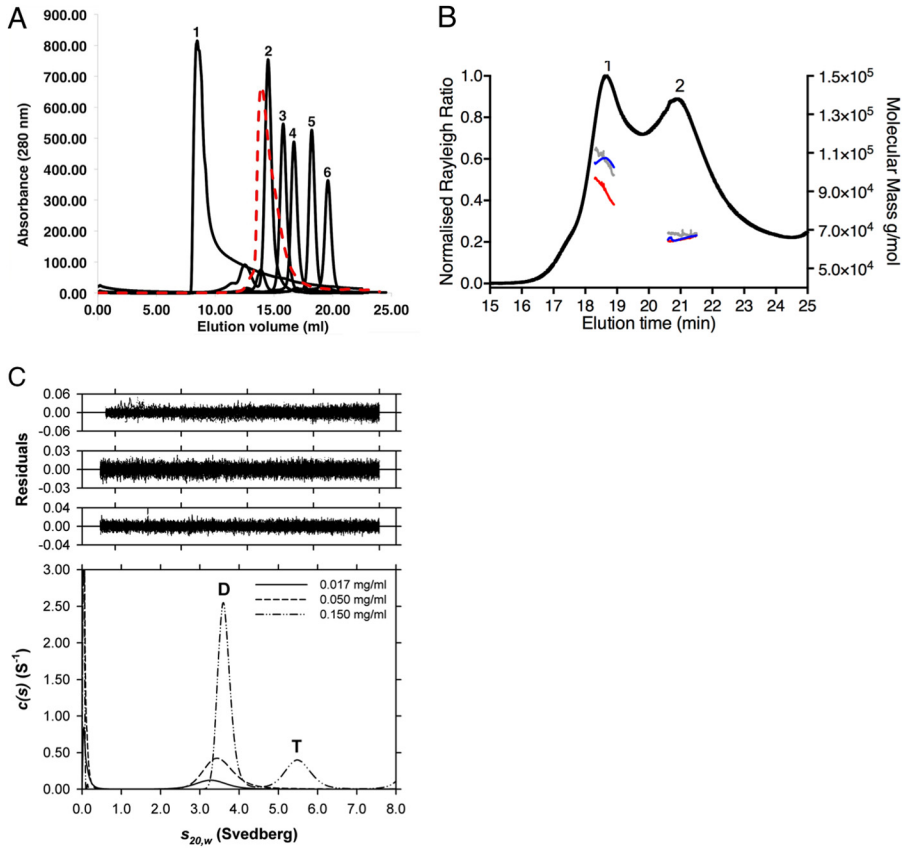

FIGURE 4. **Biophysical characterization of KIR2DL4.** *A*, size exclusion profile of purified KIR2DL4 (*red dashed line*) run on a S200 10/30 column compared with known analytical standards. Standards are as follows: BDX (2000 kDa) (*1*), conalbumin (75 kDa) (*2*), ovalbumin (44 kDa) (*3*), carbonic anhydrase (29 kDa) (*4*), ribonuclease A (13.7 kDa) (*5*), and aprotinin (6.5 kDa) (*6*). *B*, molecular mass estimations by SEC-MALS. The light scattering (at 90°) from 10 mg/ml KIR2DL4 is shown in *black*. The molecular mass estimations from three different KIR2DL4 concentrations are shown (3 mg/ml in *red*, 5 mg/ml in *gray*, and 10 mg/ml in *blue*). *C*, sedimentation velocity analysis of KIR2DL4. The continuous sedimentation coefficient (*c(s)*) distribution is plotted as a function of the standardized sedimentation coefficient for KIR2DL4 at 0.017 mg/ml (*solid line*), 0.05 mg/ml (*dashed line*), and 0.15 mg/ml (*dashed and dotted line*). The KIR2DL4 dimer and tetramer are indicated with *D* and *T*, respectively. Sedimentation velocity experiments were conducted in a Beckman model XL-I analytical ultracentrifuge as described under "Experimental Procedures." Continuous size distribution analysis was performed using the program SEDFIT at a resolution of 200, with s_{min} = 0 S, s_{max} = 8 S, and p = 0.95 (28–30).

more, Phe[34] that similarly binds the β1-β2 loop of HLA in KIR3DL1 was observed to have shifted 7.4 Å in KIR2DL4 to form an integral part of the tetramer interface (Figs. 2*B* and 3B). Clearly, by reassigning residues to forming the tetramer interface, the D0 domain of the KIR2DL4 multimer cannot engage HLA analogously to KIR3DL1.

KIR2DL4 Tetramers Do Not Interact with pHLA-Ia or HLA-G in Direct Binding Studies

To probe the interaction between KIR2DL4 and pHLA-Ia, a panel of 100 pHLA-Ia comprising HLA-A, -B, and -C was screened via a single HLA-antigen bead assay. For each of the HLAs, no binding was observed above the background level determined by the negative control (data not shown). Further, binding to HLA-G (with the peptides RIIPRHLQL and RLPKDFRIL) was assessed by surface plasmon resonance. The experiment was performed in two orientations (*i.e.* with either HLA-G (and the control HLA-B*57:01) coupled to the chip via the monoclonal antibody W6/32 or by KIR2DL4 coupled to the chip with the anti-His_6 monoclonal antibody 4D11). No interaction between KIR2DL4 and HLA-G was observed regardless of orientation (data not shown).

Biophysical Characterization of the Oligomeric State of KIR2DL4

Size Exclusion Chromatography and Dynamic Light Scattering—The tetrameric assembly observed in the crystal lattice of KIR2DL4 prompted further investigation by a number of biophysical techniques, first by analytical size exclusion chromatography performed on a Superdex S200 10/30 column equilibrated in either a buffer solution comprising 10 mM Tris, pH 8.0, and 150 mM NaCl or in a buffer comprising 10 mM citrate, pH 5.5, and 150 mM NaCl. In both running buffers, KIR2DL4 was observed to elute predominantly at a molecular weight consistent with a 100-kDa protein (14.8 ml), with a trailing edge to the elution peak consistent with a 50-kDa protein (15.2 ml) when compared with a set of known standards (Fig. 4*A*). This corresponded to protein species with molecular weights consistent with tetramers and dimers of KIR2DL4 in solution.

The molecular mass of KIR2DL4 was further analyzed using SEC-MALS. Signals from the MALS were normalized using BSA. Three different concentrations of KIR2DL4 (3, 5, and 10 mg/ml) were injected onto the column with a pore size of ~300 Å, with all three concentrations resulting in identical light scat-

tering profiles (Fig. 6). Two major peaks were observed with retention times of 18.57 and 20.80 min (Fig. 4*B*). The MALS estimated molecular mass for peak 1 at 10, 5, and 3 mg was 107.1 kDa ± 2.73%, 107.3 kDa ± 1.84%, and 97.2 kDa ± 3.34%, respectively. The MALS estimated molecular mass for peak 2 at 10, 5, and 3 mg was 64.5 kDa ± 3.33%, 67.7 kDa ± 2.27%, and 64.5 kDa ± 4.12%, respectively (Fig. 6). These molecular masses are consistent with peak 1 representing a tetramer and peak 2 representing a dimer of KIR2DL4 in solution.

Analytical Ultracentrifugation—To determine the quaternary structure of KIR2DL4 in aqueous solution, sedimentation velocity studies were performed using analytical ultracentrifugation (Table 2). Data at multiple time points generated at a rotor speed of 40,000 rpm were fitted to a continuous size distribution model (28–30). The resulting $c(s)$ distributions at initial concentrations of 0.017, 0.05, and 0.15 mg/ml are compared in Fig. 4*C*, which shows that KIR2DL4 undergoes concentration-dependent self-association. At low protein concentrations of 0.017 and 0.05 mg/ml, the protein exists as a single peak spanning a sedimentation coefficient range of 2.5–4.5 S. This suggests that KIR2DL4 exists in a rapid monomer-dimer equilibrium at low protein concentrations. However, at the higher protein concentration of 0.15 mg/ml, KIR2DL4 forms dimers (s = 3.5 S) and tetramers (s = 5.5 S). The hydrodynamic properties of the KIR2DL4 dimer and tetramer are reported in Table 2.

Small Angle X-ray Scattering—To further probe KIR2DL4 oligomerization, we performed small angle x-ray scattering analysis at a range of protein concentrations (Fig. 5, *A*–*C*). KIR2DL4 was observed to undergo a concentration-dependent increase in molecular mass, radius of gyration, and maximal particle dimension, indicating that the molecule has a propensity to oligomerize in solution (Table 3). These effects were not due to the presence of nonspecific protein aggregation, as judged by the linearity of Guinier plots (Fig. 5). At low protein concentrations (0.3 mg/ml), KIR2DL4 had a molecular mass of 49 kDa, suggesting that the predominant species present at this

TABLE 2
Hydrodynamic properties of KIR2DL4 oligomers

Oligomeric species	$s^0_{20,w}$ [a]	f/f_0 [b]
	S	
Dimer	3.6	1.3
Tetramer	5.5	1.4

[a] Standardized sedimentation coefficient obtained from the ordinate maxima of the $c(s)$ distribution peaks calculated at a KIR2DL4 concentration of 0.15 mg/ml (Fig. 1).
[b] Frictional ratio calculated using the $\bar{\nu}$ method (57).

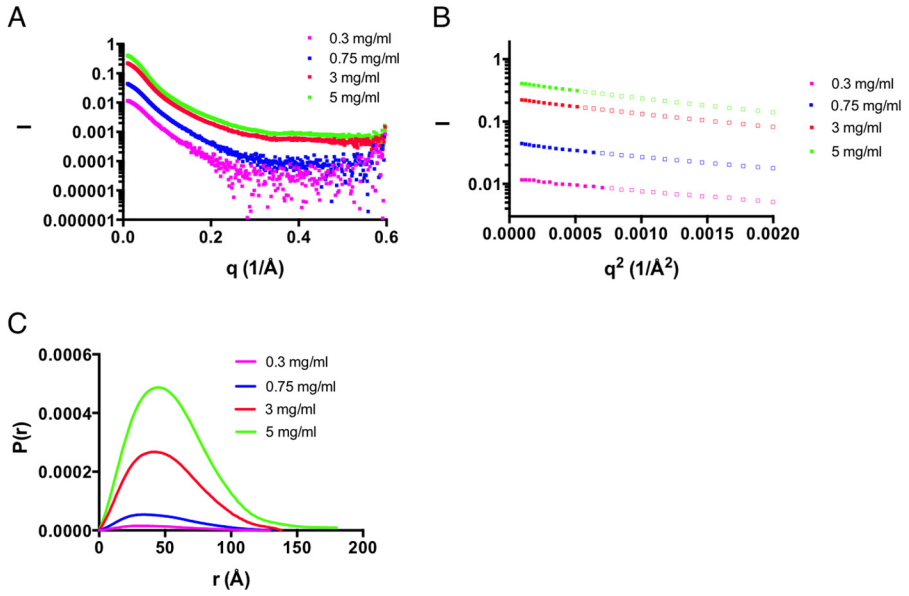

FIGURE 5. **KIR2DL4 SAXS data analysis.** *A*, raw SAXS scattering curves for KIR2DL4 recorded at a range of protein concentrations. *B*, the low angle region of the SAXS curves are represented as Guinier plots, which, for well behaving samples are linear for values of $q \leq 1/R_g$ (*filled squares*). *C*, distance distribution function. The distributions of interatomic spacings are represented as $p(r)$ plots.

TABLE 3
Summary of SAXS measurements

The radius of gyration (R_g) calculated by Guinier analysis and the indirect transfer program GNOM, the maximal particle dimension (D_{max}), molecular mass (MM) and oligomeric status of KIR2DL4 and KIR2DL2 were determined by SAXS at a range of protein concentrations. The oligomeric status was calculated by dividing the observed molecular mass by that calculated from the amino acid sequence.

Sample	Concentration	R_g, Guinier	R_g, GNOM	D_{max}	MM	Oligomeric status	$I(0)$
	mg/ml	*Å*	*Å*	*Å*	*kDa*		
KIR2DL4	0.35	36.9	37.7	129.0	49.0	1.9	0.0120
	0.75	38.8	39.1	132.3	87.0	3.3	0.044
	3	40.9	41.2	138.3	113.0	4.3	0.230
	5	42.5	45.8	159.1	125.0	4.8	0.420
KIR2DL2	0.35	29.3	22.4	71.8	25.1	1.0	0.006
	0.7	23.3	23.8	79.8	27.2	1.1	0.013
	1.4	24.3	25.2	85.4	28.3	1.2	0.027

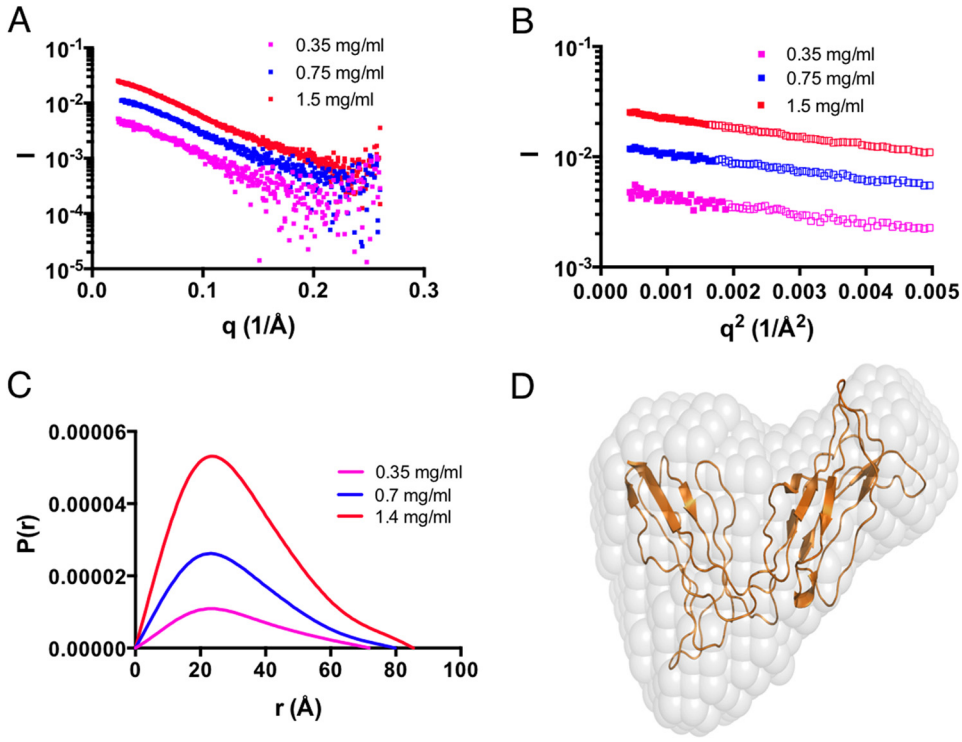

FIGURE 6. **KIR2DL2 SAXS data analysis.** *A*, raw SAXS scattering curves for KIR2DL2 recorded at a range of protein concentrations. *B*, the low angle region of the SAXS curves are represented as Guinier plots, which, for well behaving samples are linear for values of $q \leq 1/R_g$ (*filled squares*). *C*, distance distribution function. The distributions of interatomic spacings are represented as *p*(*r*) plots. *D*, DAMMIF *ab initio* model overlaid with the structure of KIR2DL2.

concentration is a dimer. At the highest concentration tested (5 mg/ml), KIR2DL4 had a molecular mass of 125 kDa, which corresponds to an oligomeric status of 4.8. Accordingly, KIR2DL4 has the capacity to form tetramers and potentially even higher order oligomers. In contrast, KIR2DL2, another two-domain KIR with a D1-D2 arrangement, has a mass (25.1–28.3 kDa) that was consistent with that predicted for a monomer (23 kDa) and did not change appreciably with increasing protein concentrations (Table 3) (Fig. 6, *A*–*C*). The *ab initio* SAXS model derived from this data overlaid well with the structure of KIR2DL2 (Fig. 6*D*), further supporting the conclusion that KIR2DL2 is monomeric in solution. Thus, our data suggest that the ability to oligomerize is not a general feature of KIRs.

To gain an insight into the shape of KIR2DL4 in solution, we performed *ab initio* modeling using the SAXS data that best correspond to the KIR2DL4 dimer (0.35 mg/ml, oligomeric status 1.9) and tetramer (3 mg/ml, oligomeric status 4.3). At 0.35 mg/ml, KIR2DL4 has a butterfly-like appearance with approximate dimensions 130 × 55 × 40 Å that overlaid well with the extended head-to-head dimer (Fig. 7*A*) but not the more compact side-by-side dimer (Fig. 7*B*). At 3 mg/ml, the KIR2DL4 SAXS envelope retains the appearance of a flattened particle but is markedly wider, with approximate dimensions of 140 × 80 × 35 Å. The 3 mg/ml SAXS model overlays reasonably well with the KIR2DL4 tetramer observed within the crystal lattice (Fig. 7*C*). Overall, our SAXS data indicate that KIR2DL4 dimerizes via D0-mediated head-to-head interactions and that tetramers and potentially larger order oligomers can be formed from the stepwise lateral association of further KIR2DL4 molecules (Fig. 7*D*).

DISCUSSION

KIR2DL4 is atypical and in comparison with other KIRs differs in manner of cellular localization, candidate ligand preference, and structure. The expression of HLA-G, a proposed ligand for KIR2DL4 (47), at the maternal-fetal interface has led to the suggestion that KIR2DL4 is involved in the maintenance of pregnancy. It is postulated that this interaction leads to the activation of NK cells and the secretion of factors that promote vascular remodeling in the uterus (48, 49). To this end, some groups have reported an interaction with HLA-G, whereas other investigations suggest that it does not (23, 24). Hence, to further understand this enigmatic molecule, we studied KIR2DL4 structurally and by a number of biophysical techniques.

We showed that, unlike other KIR receptors, KIR2DL4 oligomerizes in a concentration-dependent manner. KIR2DL4 was observed as a tetramer in the crystal lattice and in a dimer-tetramer equilibrium by SEC-MALS, SAXS, and analytical ultracentrifugation. By SAXS, the architecture of the dimer was observed to be more consistent with the crystallographic rotational dimer, raising the possibility that oligomerization may proceed by the lateral addition of rotationally related molecules in a stepwise fashion. This is driven by the association of the D0 domains.

The oligomerization is probably facilitated by key residues in the D0 domain of KIR2LD4. The unique Cys^{10}–Cys^{28} disulfide bond pairing was shown to impact the B-C and C-C′ loops at the interface of the tetramer, giving the D0 domain of KIR2DL4 a conformation that is distinct from that of KIR3DL1. Fur-

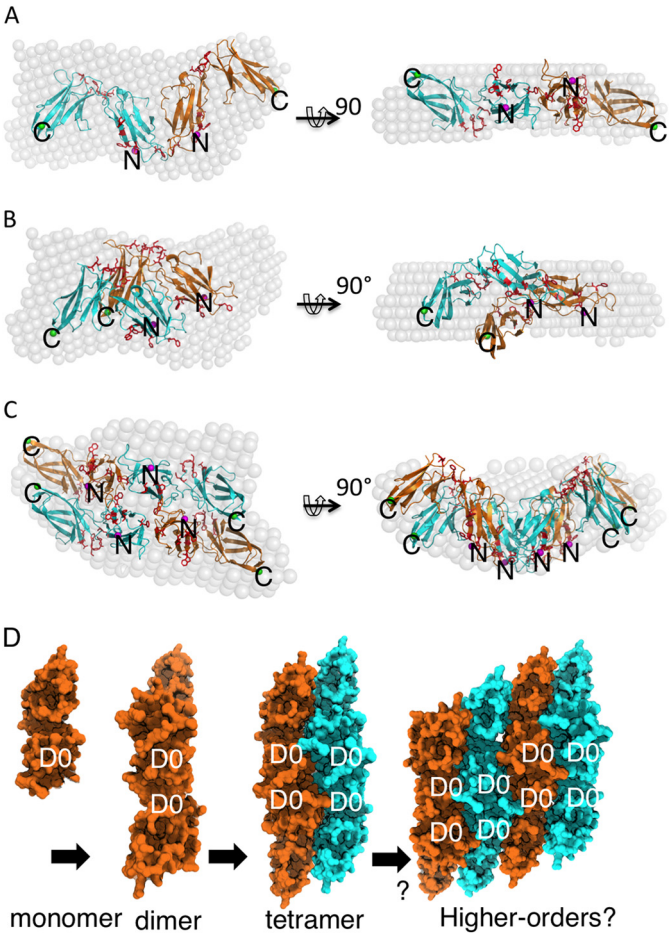

FIGURE 7. **KIR2LD4 SAXS modeling and schematic representation of oligomerization.** *A–C*, DAMMIF *ab initio* models were generated for KIR2DL4. At a concentration of 0.3 mg/ml, the KIR2DL4 oligomeric status is 1.9 (dimer), and at 3 mg/ml, the oligomeric status is 4.3 (tetramer). For *A–C*, the N termini are represented by *magenta spheres* and the letter *N*, and the C termini are shown by *green spheres* and the letter *C*. Residues that contact HLA-B*57:01 in KIR3DL1 are shown by *red sticks*. *A*, fitting the rotational dimer model at 0.3 mg/ml; *B*, fitting the translational dimer model at 0.3 mg/ml; *C*, fitting the tetramer model at 3 mg/ml; *D*, schematic representation of the oligomeric assembly of KIR2DL4. The dimer is assembled by the head-to-head association of KIR2DL4 D0 domains. The stepwise association of dimers assembles the tetramer and higher order oligomers via the D0 domains.

ther, unlike in KIR3DL1, the D0 domain of KIR2DL4 was not glycosylated. The KIR2DL4 residue (Thr^{71}) that is equivalent to the glycosylated residue on the D0 domain of KIR3DL1 (Asn^{71}) abuts the tetramerization interface such that glycosylation at this position would prevent oligomerization of the receptor.

The contribution of conserved residues that are critical to HLA binding in KIR3DL1 to forming the oligomerization interface in KIR2DL4 indicates that the D0 domain of the KIR2DL4 multimer does not bind HLA analogously to the D0-D1 arrangement in KIR3DL1. Whether the KIR2DL4 dimer or tetramer is capable of binding HLA similarly to the D1-D2 arrangement observed for KIR3DL1 and KIR2Ds remains uncertain, although modeling suggests that the docking mode would need to be distinctly different to accommodate the KIR2DL4 tetramer (data not shown). Indeed, we were unable to detect an interaction between KIR2DL4 and a panel of 100 pHLA-Ia by single HLA-antigen bead assay. Further, we were unable to detect an interaction between KIR2DL4 and HLA-G by surface plasmon resonance. Thus, as judged by direct binding investigations, KIR2DL4 does not appear to bind pHLA-I with an appreciable affinity. Certainly, further work is required to elucidate the ligand preference for the receptor. In this vein, the details of the oligomerization of the receptor will provide a base to explore the importance of self-association in regulating ligand binding.

Clues as to potential KIR2DL4 ligands may be seen in the distribution of charge across the molecule. KIR2DL4 has a dipolar charge distribution with the D0 domain carrying an overall electropositive net charge such that the association of these domains in the tetramer forms a large positively charged patch. This is in keeping with the KIR2DL4 D0 domain being the proposed binding site for the negatively charged HSPG (25). The report of HSPG binding to KIR2LD4 is in line with similar studies on the natural cytotoxicity receptors NKp30, NKp44, and NKp46 (50, 51). Similar to this, the positive charge on the KIR3DL2, KIR3DL1/S1, and KIR2DL4 D0 domains has been proposed to act as a pattern recognition motif in the binding of CpG oligodeoxynucleotide (52). Presumably, the role of the D0 domain in these interactions is to provide charge complementarity with the ligands. However, the specificity of the interactions and the role of the other KIR domains are not yet clear. It remains to be substantiated whether HSPG is a functional KIR2LD4 ligand and how specificity for the interaction is achieved.

Oligomerization of KIR2DL4 may be an important mechanism for regulating signal transduction. KIR2DL4 possesses both activating and inhibitory signaling domains. The cytoplasmic immunoreceptor tyrosine-based inhibition motif domain has been reported to elicit functional inhibitory signals (15, 53). However, intracellular KIR2DL4 signaling appears to be predominantly activating, via recruitment of the FcεR-γ adaptor, resulting in a proinflammatory response characterized by IFN-γ secretion and minimal cytotoxicity (34, 54, 55). Indeed, it has been suggested that vascular remodeling in the uterus during early pregnancy is a result of NK cell senescence from prolonged activatory signaling through KIR2DL4 (49). Whether inhibitory signaling through KIR2DL4 is physiologically significant and whether there is a balance between activating and inhibitory signaling remains unknown. However, oligomerization of the receptor may provide an important means for regulating signal output, by either sequestering or concentrating local regions for adaptor protein and signaling protein binding. Further, the ability of KIR2DL4 to recruit signaling proteins to the endosome may provide a scaffold to regulate NK cell signal transduction in isolation from the cell surface (56). Whether KIR2DL4 functions as an immunoregulatory scaffold protein and the role of self-association in coordinating signaling are questions that remain to be answered.

Acknowledgments—Crystallization experiments were performed at the Monash Macromolecular Crystallization Facility (Monash University, Victoria, Australia). This research was undertaken in part on the MX2 and SAXS/WAXS beamlines at the Australian Synchrotron (Victoria, Australia).

REFERENCES

1. Jost, S., and Altfeld, M. (2013) Control of human viral infections by natural killer cells. *Annu. Rev. Immunol.* **31,** 163–194
2. Costello, R. T., Sivori, S., Marcenaro, E., Lafage-Pochitaloff, M., Mozziconacci, M. J., Reviron, D., Gastaut, J. A., Pende, D., Olive, D., and Moretta, A. (2002) Defective expression and function of natural killer cell-triggering receptors in patients with acute myeloid leukemia. *Blood* **99,** 3661–3667
3. Raffaghello, L., Prigione, I., Airoldi, I., Camoriano, M., Levreri, I., Gambini, C., Pende, D., Steinle, A., Ferrone, S., and Pistoia, V. (2004) Downregulation and/or release of NKG2D ligands as immune evasion strategy of human neuroblastoma. *Neoplasia* **6,** 558–568
4. Liu, J., Xiao, Z., Ko, H. L., Shen, M., and Ren, E. C. (2014) Activating killer cell immunoglobulin-like receptor 2DS2 binds to HLA-A*11. *Proc. Natl. Acad. Sci. U.S.A.* **111,** 2662–2667
5. Saulquin, X., Gastinel, L. N., and Vivier, E. (2003) Crystal structure of the human natural killer cell activating receptor KIR2DS2 (CD158j). *J. Exp. Med.* **197,** 933–938
6. Graef, T., Moesta, A. K., Norman, P. J., Abi-Rached, L., Vago, L., Older Aguilar, A. M., Gleimer, M., Hammond, J. A., Guethlein, L. A., Bushnell, D. A., Robinson, P. J., and Parham, P. (2009) KIR2DS4 is a product of gene conversion with KIR3DL2 that introduced specificity for HLA-A*11 while diminishing avidity for HLA-C. *J. Exp. Med.* **206,** 2557–2572
7. Maenaka, K., Juji, T., Stuart, D. I., and Jones, E. Y. (1999) Crystal structure of the human p58 killer cell inhibitory receptor (KIR2DL3) specific for HLA-Cw3-related MHC class I. *Structure* **7,** 391–398
8. Boyington, J. C., Motyka, S. A., Schuck, P., Brooks, A. G., and Sun, P. D. (2000) Crystal structure of an NK cell immunoglobulin-like receptor in complex with its class I MHC ligand. *Nature* **405,** 537–543
9. Fan, Q. R., Long, E. O., and Wiley, D. C. (2001) Crystal structure of the human natural killer cell inhibitory receptor KIR2DL1-HLA-Cw4 complex. *Nat. Immunol.* **2,** 452–460
10. Vivian, J. P., Duncan, R. C., Berry, R., O'Connor, G. M., Reid, H. H., Beddoe, T., Gras, S., Saunders, P. M., Olshina, M. A., Widjaja, J. M., Harpur, C. M., Lin, J., Maloveste, S. M., Price, D. A., Lafont, B. A., McVicar, D. W., Clements, C. S., Brooks, A. G., and Rossjohn, J. (2011) Killer cell immunoglobulin-like receptor 3DL1-mediated recognition of human leukocyte antigen B. *Nature* **479,** 401–405
11. Finton, K. A., and Strong, R. K. (2012) Structural insights into activation of antiviral NK cell responses. *Immunol. Rev.* **250,** 239–257
12. O'Connor, G. M., Vivian, J. P., Widjaja, J. M., Bridgeman, J. S., Gostick, E., Lafont, B. A., Anderson, S. K., Price, D. A., Brooks, A. G., Rossjohn, J., and McVicar, D. W. (2014) Mutational and structural analysis of KIR3DL1 reveals a lineage-defining allotypic dimorphism that impacts both HLA and peptide sensitivity. *J. Immunol.* **192,** 2875–2884
13. McVicar, D. W., and Burshtyn, D. N. (2001) Intracellular signaling by the killer immunoglobulin-like receptors and Ly49. *Sci. STKE* **2001,** re1
14. Burshtyn, D. N., Scharenberg, A. M., Wagtmann, N., Rajagopalan, S., Berrada, K., Yi, T., Kinet, J. P., and Long, E. O. (1996) Recruitment of tyrosine phosphatase HCP by the killer cell inhibitor receptor. *Immunity* **4,** 77–85
15. Faure, M., and Long, E. O. (2002) KIR2DL4 (CD158d), an NK cell-activating receptor with inhibitory potential. *J. Immunol.* **168,** 6208–6214
16. Kikuchi-Maki, A., Catina, T. L., and Campbell, K. S. (2005) Cutting edge: KIR2DL4 transduces signals into human NK cells through association with the Fc receptor γ protein. *J. Immunol.* **174,** 3859–3863
17. Rajagopalan, S. (2010) Endosomal signaling and a novel pathway defined by the natural killer receptor KIR2DL4 (CD158d). *Traffic* **11,** 1381–1390
18. Moesta, A. K., Norman, P. J., Yawata, M., Yawata, N., Gleimer, M., and Parham, P. (2008) Synergistic polymorphism at two positions distal to the ligand-binding site makes KIR2DL2 a stronger receptor for HLA-C than KIR2DL3. *J. Immunol.* **180,** 3969–3979
19. Gumperz, J. E., Barber, L. D., Valiante, N. M., Percival, L., Phillips, J. H., Lanier, L. L., and Parham, P. (1997) Conserved and variable residues within the Bw4 motif of HLA-B make separable contributions to recognition by the NKB1 killer cell-inhibitory receptor. *J. Immunol.* **158,** 5237–5241
20. Hansasuta, P., Dong, T., Thananchai, H., Weekes, M., Willberg, C., Aldemir, H., Rowland-Jones, S., and Braud, V. M. (2004) Recognition of HLA-A3 and HLA-A11 by KIR3DL2 is peptide-specific. *Eur. J. Immunol.* **34,** 1673–1679
21. Rajagopalan, S., Bryceson, Y. T., Kuppusamy, S. P., Geraghty, D. E., van der Meer, A., Joosten, I., and Long, E. O. (2006) Activation of NK cells by an endocytosed receptor for soluble HLA-G. *PLoS Biol.* **4,** e9
22. Clements, C. S., Kjer-Nielsen, L., Kostenko, L., Hoare, H. L., Dunstone, M. A., Moses, E., Freed, K., Brooks, A. G., Rossjohn, J., and McCluskey, J. (2005) Crystal structure of HLA-G: a nonclassical MHC class I molecule expressed at the fetal-maternal interface. *Proc. Natl. Acad. Sci. U.S.A.* **102,** 3360–3365
23. Boyson, J. E., Erskine, R., Whitman, M. C., Chiu, M., Lau, J. M., Koopman, L. A., Valter, M. M., Angelisova, P., Horejsi, V., and Strominger, J. L. (2002) Disulfide bond-mediated dimerization of HLA-G on the cell surface. *Proc. Natl. Acad. Sci. U.S.A.* **99,** 16180–16185
24. Le Page, M. E., Goodridge, J. P., John, E., Christiansen, F. T., and Witt, C. S. (2014) Killer Ig-like receptor 2DL4 does not mediate NK cell IFN-γ responses to soluble HLA-G preparations. *J. Immunol.* **192,** 732–740
25. Brusilovsky, M., Cordoba, M., Rosental, B., Hershkovitz, O., Andrake, M. D., Pecherskaya, A., Einarson, M. B., Zhou, Y., Braiman, A., Campbell, K. S., and Porgador, A. (2013) Genome-wide siRNA screen reveals a new cellular partner of NK cell receptor KIR2DL4: heparan sulfate directly modulates KIR2DL4-mediated responses. *J. Immunol.* **191,** 5256–5267
26. Stifter, S. A., Gould, J. A., Mangan, N. E., Reid, H. H., Rossjohn, J., Hertzog, P. J., and de Weerd, N. A. (2014) Purification and biological characterization of soluble, recombinant mouse IFNβ expressed in insect cells. *Protein Expr. Purif.* **94,** 7–14
27. Aricescu, A. R., Lu, W., and Jones, E. Y. (2006) A time- and cost-efficient system for high-level protein production in mammalian cells. *Acta Crystallogr. D Biol. Crystallogr.* **62,** 1243–1250
28. Perugini, M. A., Schuck, P., and Howlett, G. J. (2000) Self-association of human apolipoprotein E3 and E4 in the presence and absence of phospholipid. *J. Biol. Chem.* **275,** 36758–36765
29. Schuck, P. (2000) Size-distribution analysis of macromolecules by sedimentation velocity ultracentrifugation and Lamm equation modeling. *Biophys. J.* **78,** 1606–1619
30. Schuck, P., Perugini, M. A., Gonzales, N. R., Howlett, G. J., and Schubert, D. (2002) Size-distribution analysis of proteins by analytical ultracentrifugation: strategies and application to model systems. *Biophys. J.* **82,** 1096–1111
31. Clements, C. S., Kjer-Nielsen, L., Kostenko, L., McCluskey, J., and Rossjohn, J. (2006) The production, purification and crystallization of a soluble form of the nonclassical MHC HLA-G: the essential role of cobalt. *Acta Crystallogr. Sect. F Struct. Biol. Cryst. Commun.* **62,** 70–73
32. Saunders, P. M., Vivian, J. P., Baschuk, N., Beddoe, T., Widjaja, J., O'Connor, G. M., Hitchen, C., Pymm, P., Andrews, D. M., Gras, S., McVicar, D. W., Rossjohn, J., and Brooks, A. G. (2015) The interaction of KIR3DL1*001 with HLA class I molecules is dependent upon molecular microarchitecture within the Bw4 epitope. *J. Immunol.* **194,** 781–789
33. Parham, P., Barnstable, C. J., and Bodmer, W. F. (1979) Use of a monoclonal antibody (W6/32) in structural studies of HLA-A,B,C, antigens. *J. Immunol.* **123,** 342–349
34. Rajagopalan, S., Fu, J., and Long, E. O. (2001) Cutting edge: induction of IFN-γ production but not cytotoxicity by the killer cell Ig-like receptor KIR2DL4 (CD158d) in resting NK cells. *J. Immunol.* **167,** 1877–1881
35. Goding, J. W. (1996) *Monoclonal Antibodies: Principles and Practice*, Chapter 10, pp. 234–326, Elsevier Science, Amsterdam
36. Semenyuk, A. V., and Svergun, D. I. (1991) GNOM: a program package for small-angle scattering data processing. *J. Appl. Crystallogr.* **24,** 537–540
37. Franke, D., and Svergun, D. I. (2009) DAMMIF, a program for rapid *ab-initio* shape determination in small-angle scattering. *J. Appl. Crystallogr.* **42,** 342–346
38. Collaborative Computational Project, Number 4 (1994) The CCP4 suite: programs for protein crystallography. *Acta Crystallogr. D Biol. Crystallogr.* **50,** 760–763
39. Evans, P. (2006) Scaling and assessment of data quality. *Acta Crystallogr. D Biol. Crystallogr.* **62,** 72–82
40. Leslie, A. G. W. (1992) Recent changes to the MOSFLM package for process-

ing film and image plate data. *Joint CCP4 + ESF-EAMCB Newsletter on Protein Crystallography*, Number 26, Daresbury Laboratory, Warrington, UK
41. McCoy, A. J., Grosse-Kunstleve, R. W., Adams, P. D., Winn, M. D., Storoni, L. C., and Read, R. J. (2007) Phaser crystallographic software. *J. Appl. Crystallogr.* **40,** 658–674
42. Emsley, P., and Cowtan, K. (2004) Coot: model-building tools for molecular graphics. *Acta Crystallogr. D Biol. Crystallogr.* **60,** 2126–2132
43. Adams, P. D., Afonine, P. V., Bunkóczi, G., Chen, V. B., Davis, I. W., Echols, N., Headd, J. J., Hung, L. W., Kapral, G. J., Grosse-Kunstleve, R. W., McCoy, A. J., Moriarty, N. W., Oeffner, R., Read, R. J., Richardson, D. C., Richardson, J. S., Terwilliger, T. C., and Zwart, P. H. (2010) PHENIX: a comprehensive Python-based system for macromolecular structure solution. *Acta Crystallogr. D Biol. Crystallogr.* **66,** 213–221
44. Chen, V. B., Arendall, W. B., 3rd, Headd, J. J., Keedy, D. A., Immormino, R. M., Kapral, G. J., Murray, L. W., Richardson, J. S., and Richardson, D. C. (2010) MolProbity: all-atom structure validation for macromolecular crystallography. *Acta Crystallogr. D Biol. Crystallogr.* **66,** 12–21
45. Halaby, D. M., Poupon, A., and Mornon, J. (1999) The immunoglobulin fold family: sequence analysis and 3D structure comparisons. *Protein Eng.* **12,** 563–571
46. Lawrence, M. C., and Colman, P. M. (1993) Shape complementarity at protein/protein interfaces. *J. Mol. Biol.* **234,** 946–950
47. Rajagopalan, S., and Long, E. O. (2012) KIR2DL4 (CD158d): An activation receptor for HLA-G. *Front. Immunol.* **3,** 258
48. Rajagopalan, S. (2014) HLA-G-mediated NK cell senescence promotes vascular remodeling: implications for reproduction. *Cell. Mol. Immunol.* **11,** 460–466
49. Rajagopalan, S., and Long, E. O. (2012) Cellular senescence induced by CD158d reprograms natural killer cells to promote vascular remodeling. *Proc. Natl. Acad. Sci. U.S.A.* **109,** 20596–20601
50. Bloushtain, N., Qimron, U., Bar-Ilan, A., Hershkovitz, O., Gazit, R., Fima, E., Korc, M., Vlodavsky, I., Bovin, N. V., and Porgador, A. (2004) Membrane-associated heparan sulfate proteoglycans are involved in the recognition of cellular targets by NKp30 and NKp46. *J. Immunol.* **173,** 2392–2401
51. Hecht, M. L., Rosental, B., Horlacher, T., Hershkovitz, O., De Paz, J. L., Noti, C., Schauer, S., Porgador, A., and Seeberger, P. H. (2009) Natural cytotoxicity receptors NKp30, NKp44 and NKp46 bind to different heparan sulfate/heparin sequences. *J. Proteome Res.* **8,** 712–720
52. Sivori, S., Falco, M., Carlomagno, S., Romeo, E., Soldani, C., Bensussan, A., Viola, A., Moretta, L., and Moretta, A. (2010) A novel KIR-associated function: evidence that CpG DNA uptake and shuttling to early endosomes is mediated by KIR3DL2. *Blood* **116,** 1637–1647
53. Cantoni, C., Verdiani, S., Falco, M., Pessino, A., Cilli, M., Conte, R., Pende, D., Ponte, M., Mikaelsson, M. S., Moretta, L., and Biassoni, R. (1998) p49, a putative HLA class I-specific inhibitory NK receptor belonging to the immunoglobulin superfamily. *Eur. J. Immunol.* **28,** 1980–1990
54. Kikuchi-Maki, A., Yusa, S., Catina, T. L., and Campbell, K. S. (2003) KIR2DL4 is an IL-2-regulated NK cell receptor that exhibits limited expression in humans but triggers strong IFN-γ production. *J. Immunol.* **171,** 3415–3425
55. Goodridge, J. P., Witt, C. S., Christiansen, F. T., and Warren, H. S. (2003) KIR2DL4 (CD158d) genotype influences expression and function in NK cells. *J. Immunol.* **171,** 1768–1774
56. Shaw, A. S., and Filbert, E. L. (2009) Scaffold proteins and immune-cell signalling. *Nat. Rev. Immunol.* **9,** 47–56
57. Laue, T. M., Shah, B. D., Ridgeway, T. M., Pelletier, S. L. (1991) in *Analytical Ultracentrifugation in Biochemistry and Polymer Science*, pp. 90–125, Royal Society of Chemistry, London
58. Brown, P. H., Balbo, A., and Schuck, P. (2007). Using prior knowledge in the determination of macromolecular size distributions by analytical ultracentrifugation. *Biomacromolecules* **8,** 2011–2024